PCCP

Accepted Manuscript

ROYAL SOCIETY OF CHEMISTRY

www.rsc.org/pccp

Grain-size Dependence of Mechanical Properties in Polycrystalline Boron-Nitride: A Computational Study

Matthew Becton and Xianqiao Wang
College of Engineering, University of Georgia, Athens, GA 30602

Abstract

The field of research in polycrystalline hexagonal boron nitride (PBN) has been enjoying extraordinary growth recently, in no small part due to the rise of graphene and the technical advancement of mass production in polycrystalline 2D materials. However, as the grain size in 2D materials can strongly affect their materials properties and the performance of their relevant devices, it is highly desirable to investigate this effect in PBN and leverage the service capability of PBN-based devices. Here we employ molecular dynamics simulations to explore the effects of grain size in PBN on its mechanical properties such as Young's modulus, yield strength, toughness, and energy release rate as well as its failure mechanism. By visualizing and comparing the tensile failure of PBN with and without a predefined crack we have shown that the grain size of PBN is positively correlated with its elastic modulus, yield strength and toughness. Through inclusion of a crack with varying length in the PBN samples, the energy release rate is determined for each grain size of PBN and it is concluded that the energy release rate increases with an increase in the average grain size of PBN. These findings offer useful insights into utilizing PBN for mechanical design in composite materials, abrasion resistance, and electronic devices etc.

1 Introduction

The characteristics of individual grains in polycrystalline materials have an enormous impact on their overall physical properties[1]. For two dimensional materials, the boundaries and sizes of the individual grains are not only more easily investigable, but the line-like quality of the grain boundaries grants variation in mechanical properties unable to be found in traditional three dimensional materials[2]. Of the many kinds of 2D materials currently drawing attention, hexagonal boron nitride has become the topic of research due to its structural equivalency to graphene and outstanding properties. Hexagonal boron nitride is an atomic lattice structure similar to graphene, but composed of the heterogeneous atoms boron and nitrogen in place of

carbon. This material has been garnering attention at an unprecedented rate due to its noteworthy mechanical [3-6], thermodynamic [7-9], chemical [10-12], and electronic [13, 14] properties. The mechanical stability combined with h-BN's natural sliding has endowed its fantastical applications in bulk lubrication for decades; however with the explosive growth of interest in many disparate 2D materials[15], focus has shifted towards the applicability of h-BN at the nano-level, such as an insulator used as a foil to the conductor graphene[16], a spin-filter for spintronic devices[14, 17, 18], and a nanoscale filler as a strengthening component in ceramic composite materials[19].

Technological applications require the ability to scalably produce large-area sheets beyond the micrometer-size samples of boron nitride. However, statistical physics arguments suggest that crystalline order in 2D materials is highly susceptible to various types of fluctuation and disorders, thereby hindering the mass production of high-quality single crystalline boron nitride. In practice, typical large sheets of hexagonal BN produced by chemical vapor deposition are polycrystalline, which is composed of single-crystalline domains of varying lattice orientations. Rotational disorder of polycrystalline materials leads to the presence of grain boundaries – interfaces between single-crystalline domains. Grain boundaries, a class of topological defects, are intrinsic to polycrystalline materials and inevitably affect all properties of the materials of interest. Polycrystalline boron nitride has demonstrated several physical characteristics stemming from the defects at the grain boundaries which distinguish it from pristine BN, including decreased thermal conductivity,[20-22] interesting electronic properties[23-27], lower mechanical strength[28-31], increased reactivity[32], and increased flaw tolerance[33]. As producing pristine BN requires more cost, time, and effort than massively producing PBN from milling methods, there is a burgeoning market for BN's patchwork cousin, especially if the strength, thermal, and electrical properties can be improved and controlled[34]. Therefore investigating the mechanical properties of PBN in order to better understand the use of this material will be the focus of this paper.

In the field of nanoscale simulation, it is important for the subject to be as similar as possible to the real object within simulational constraints. Towards this end we follow a simple method of generating a realistic sample of PBN. As BN is a crystalline material with a structure akin to graphene, simulational samples are generated via relatively simple algorithms[35]. However, when trying to represent polycrystalline materials realistically this simple process becomes

exponentially more difficult, as algorithmically-generated samples may not be stable or even feasibly formed under realistic conditions. Simulating the creation process of PBN also has its own difficulties, both in terms of computational resources and determining an appropriate potential. The annealing process allows for algorithmically-generated samples to better emulate experimental work and become more stable while using minimal computational resources, as opposed to the resource-consuming task of modeling realistic PBN grain growth. In this work we utilize molecular dynamics simulations to examine the mechanical properties of generated PBN samples of varying grain sizes. After discussing the visual and energetic changes in structure due to tension, we turn our attention to the property of mechanical strength. For each grain size, tensile tests are performed on annealed samples of flawed and unflawed PBN, and the results are subsequently compared and discussed.

2 Computational Models and Methods

First, an originally developed program based on the Voronoi cell method is utilized in order to generate a polycrystalline hexagonal lattice with the specific grain size of interest. The atoms in two sub-lattices are labeled atom α and β alternately. Following this, an annealing process is performed as described in our previous work [36], by utilizing the AIREBO potential for carbon, as both α and β atoms are populated by carbon atoms. After the annealing process, the α atoms are designated to be boron, and the β atoms designated to be nitrogen, forming a realistic and stable polycrystalline boron nitride test sample. In what follows, molecular dynamics simulations based on the open source code LAMMPS[37] are employed to perform the tensile and fracture simulations of PBN. In order to accurately capture the behavior of PBN, the Tersoff potential is utilized, which takes the form

$$E = \frac{1}{2}\sum_i \sum_{j \neq i} f_C(r_{ij})[f_R(r_{ij}) + b_{ij} f_A(r_{ij})] \quad (1)$$

where f_R is a repulsive two-body term while f_A is an attractive three-body term managed by the b_{ij} bond function. The parameters of the Tersoff potential utilized here for BN were documented by Matsunaga[38]; the expanded potential and all parameters are documented in the Supplementary Material Equations S1-S6 and Table S1. After the formation of PBN from the technique used with graphene, the sample is then minimized using the conjugate gradients method in order to stabilize the PBN.

The (h-BN) types tested in this paper are pristine BN and PBN. For the tensile tests, the sample is set up as shown in Figure 1. The simulated sample is a 24 nm x 24 nm square sheet under NVT ensemble using a Nose-Hoover thermostat to control temperature and standard velocity-Verlet time integration with a timestep of 1fs in order to preserve a balance between accuracy and computational cost; the pressure was not controlled. The grain sizes (referred to as g) tested in this work are (on average) 3, 4, 6, 8, 12, and 24 nm (with 24 nm grain size analogous to pristine BN). In this manner the number of grains across the sample is an integer ranging from 8 to 1 with each sample having a normally distributed size about the average grain size g; the BN grains are generated using a Voronoi cell method. In this work, the initial plane of the nanosheet is considered to be the $x - y$ plane, and perpendicular to the nanosheet is the z direction. Each grain is given a random orientation while lying in the x-y plane, so as to best mimic the orientation of disparate grains in a CVD-grown sheet of PBN. The number of atoms varies slightly due to the presence or absence of grain boundaries, but all structures have approximately 22,000 atoms, with a variance of less than 3%. The boundaries are aperiodic so as to prevent interference in the sample, and a randomized initial velocity is applied to each atom in accordance with the sample temperature with sum zero linear and angular momenta. The sample then undergoes energy minimization following the Polak-Ribiere conjugate gradients method until the relative energy difference between successive steps is less than 10^{-20}.

Before tension, the samples are completely relaxed so that there is minimal prestress inside the sample. The tensile test process is as follows: for both the pristine and polycrystalline samples the energy-minimized BN structure is kept at 1 K using Nosé-Hoover thermostatting, so as to minimize the effects of the randomized temperature profile. A timestep of 1 fs is used with the velocity-Verlet integration algorithm in order to provide a good compromise between efficiency and accuracy. In order to provide the tensile force to the sample one side of the sample is fixed in place, while the other is pulled using steered molecular dynamics using a spring constant of 100 eV/Å^2. The pulling speed is 2.5 nm/ns, as this pulling speed is slow enough to have negligible velocity-dependent effects, as shown in the supplementary information Figures S1 and S2, which indicates that, the mechanical properties of PBN, such as Young's modulus, yield strength, and toughness, are barely affected by the pulling speeds when it is equal or below 2.5 nm/ns while high pulling speeds deviate the results considerably from those with slow pulling speeds.. The results of the tests are then compiled and analyzed.

3 Results and Discussions

3.1 Mechanical properties vs. grain size

Similar to most other polycrystalline materials, the average size of the crystalline grains has a significant effect on the mechanical properties of PBN. In accordance with previous results [4], PBN with smaller grain size exhibits a lower ultimate strength and Young's Modulus, as can be confirmed from Figure 2. This is in accordance with the properties of the similar yet homogeneous material graphene, where a lower Young's Modulus and ultimate strength are expected for smaller grain sizes [36]. From Figure 3, while the tensile strength does indeed increase with grain size, there is a slight but noticeable decrease in the ultimate strain of PBN as the average size of the grains increases. In order to make the relationship between mechanical properties and grain size more clear, the data fitting with suitable curves are performed to analyze the simulation results. From the graph, the relationship between grain size and tensile strength of PBN can be expressed as $\sigma_y = 12.146 * \ln(g) + 29.976$. This positive correlation between yield strength and grain size is expected, as smaller grains equate to a larger areal percentage of grain boundaries in the sample. These grain boundaries are by definition not as stable as the pristine crystalline lattice, and thus a large number of grain boundaries create a sample with a lesser yield strength. However, an increased number of grain boundaries, while denigrating the integrity and strength of the pristine crystalline material, also allows for a greater amount of deformation before the critical failure. This phenomenon can be confirmed from the data of the maximum strain the samples can sustain, which yields the relationship between the strain and the grain size of PBN as $\varepsilon_y = -0.035 * \ln(g) + 0.4132$. For both of the curves fitted to the data of interest, the logarithmic curve has the lowest r^2 value. This can be explained by reason of the size of the grains being too small to be described by the classical Hall-Petch effect[39], and instead relying on the dependence of the work done on polycrystalline thin films to the natural log of the grain size[40].

While PBN cannot compete with polycrystalline graphene in terms of Young's modulus, there is a commonality wherein samples with smaller average grain size are less stiff; that is the Young's Modulus (E) increases with grain size as can be seen in Figure 4. The Young's Modulus is a good metric to indicate the amount of elastic deformation caused to a sample at low strain, which

is extremely useful for determining the potential working conditions of a new material. Using the slope of the initial elastic portion of the stress strain curve, the Young's Modulus is determined for each sample with a certain grain size of interest, and a trend determined. Via curve fitting the data yields the relationship $E = 54.368 * \ln(g) + 71.301$. This strong relationship between grain size and elastic modulus clearly indicates that the smaller grain size the sample has, the lower Young's modulus the sample possesses. This relationship may be explained as follows: samples with large grains are by percentage composed of more pristine crystal and less grain boundary than samples with small grain sizes, and as the grain size increases, the Young's modulus of the polycrystalline sample becomes closer to that of the pristine crystal. Similar to the relationship between the grain size and ultimate strength of PBN, the grain boundaries create a weakness which leads to a lower Young's Modulus since a larger percentage of the sample is composed of grain boundaries.

However, when it comes to toughness (T), the fragility of the grain boundaries of PBN shows a distinct comparison with the behavior of polycrystalline graphene. Toughness is a measurement of the amount of energy a material can absorb before failure; as such it can be calculated by integrating the stress-strain curve of the material and converting to the appropriate units. Figure 5 illustrates the toughness of each PBN sample, which shows a positive correlation with grain size, denoted by the equation $T = 1.4022 * \ln(g) + 3.7282$, which is the curve fitted to the toughness plot in Figure 5. Although polycrystalline graphene shows a negative correlation between grain size and toughness [36], the more brittle nature of PBN fracture induces a lesser toughness when the grain sizes are small, due to the increased probability of a grain boundary failure. In order to better understand the mechanical behavior of PBN, and its potential usage in strengthening polymer composite materials, it is crucial to also investigate the failure mechanisms of PBN.

3.2 Failure mechanism vs. grain size

In accordance with the change in mechanical properties with the decrease of the grain size as demonstrated previously, it is reasonable to investigate the failure mode of various grain sizes of PBN. Classically, PBN shows a lower strength and a larger strain at failure when compared with BN. This is expected, and supported by previous literature [4]. Unlike graphene [36], BN is a more brittle material and thus has a tendency to fail in a more spectacular fashion, as can be seen in Figure 6 where the rupture of pristine BN during tension is shown. For each of the samples tested

for the pure tensile tests (i.e. no induced flaw in the samples) the failure mechanism is sudden rupture and destruction of the PBN, as evidenced by the sharp cutoff at the end of the stress/strain curves shown in Figure 2. The stress of the sample amplifies during the tension and is concentrated at specific points along the grain boundary, as evidenced by the stress in a single grain of 3 nm grain PBN shown in Figure 7. The stress field is intensified at the connections between B and N, where bonds are formed between grains, as illustrated by the stress concentration shown in Figure 8. In polycrystalline materials, grain boundaries are formed when two or more homogeneous yet misaligned pristine crystal lattices are bonded to each other. As the crystal lattices do not align perfectly, many defects will appear along the grain boundaries, including atom vacancies, adatoms, and heteroelemental bonds. These defects act in concert to cause the stress buildup seen in Figure 8, as there are limited places where the grains are bonded to one another.

At grain boundaries, the 1:1 stoichiometry of BN is skewed such that local areas may be polarized; that is, the heterogeneity of BN ensures that at grain boundaries, there will be areas where the B-N connection is preserved, but also instances where B-B or N-N situations occur. These connections are relatively fragile, and are unable to support much tensile stress, leading to debonding of the homoelemental bonds as described previously by Mortazavi and Cuniberi [4]. This process can be observed in more detail by comparing the stress of Figure 8 to the atomic species shown in Figure 9. This dissociation of the homoelemental bonds leads to stress concentration in the remaining heteroelemental B-N bonds. Because of the relatively few, highly stress-concentrated connections between grains, when one part fails the rest fails in a rapid and spectacular fashion. Regardless of grain size, there is very little change in the sudden failure behavior demonstrated for PBN, which begins at a grain boundary and rapidly expands. This sudden failure behavior stems from the intermittent bonds at grain boundaries induced by the heterogeneity of BN, as described previously. This tendency for relatively weak grain boundaries induces a sudden failure reminiscent of brittle materials, where a single weak point failing causes a very fast chain reaction without the semi-fluidity exhibited by ductile materials. To better study the effect of a ‘weak point’ in this material, the behavior of PBN with regard to induced defects is tested and discussed in what follows.

A predefined crack in the pristine BN sheet provides an area for stress to concentrate, invariably causing fracture to proceed from this point. Interestingly, where an unflawed pristine sheet fails dramatically after reaching failure, the flawed sheet has a much slower rate of failure, as the amount of strain energy in the sheet has not built up to nearly the same amount. The large energy release at failure can cause destruction of the crystal lattice surrounding the failure point at excessively high stresses, so the fracture at relatively low stress caused by the induced crack leads to slow, controlled tearing as evidenced by the more gradual decline in stress after failure in Figure 10. Fracture initiates at the edge defect, and then generally travels across grain boundaries (GB) perpendicular to the direction of fracture, but if close enough to a GB which runs along a similar direction the fracture shifts to the grain boundary and propagates from there, as seen in Figure 12. Figure 12 shows atoms only with a potential energy between -7 and -9 eV, such that only grain boundaries, edges, and heavily stressed atoms are in the picture. This intriguing plot makes it easy to see the propagation of the fracture, the associated grain boundaries, and the build-up and release of stress during the fracture process. For the purpose of illustration, the 1 nm long crack in the 8 nm grain size PBN begins to propagate in the center of the lower-middle grain. The crack then crosses over into the central grain and finally extends along a grain boundary in the upper portion of the image.

The progression of crack formation in a material provides a useful avenue to estimate its resistance to defects, and can be evaluated by the energy release rate of the material. From the difference in toughness exhibited by the various initial induced crack lengths, the energy release rate (G) of the material can be calculated. The toughness of the sample is a metric of the energy absorbed by the sample before failure. The energy release rate is the amount of energy able to be dissipated during fracture per unit length of fracture. It can be calculated as $G = -\frac{\partial(U-V)}{\partial L}$, where U is the potential energy available for crack growth, V is the work done by external forces (here the stress due to tension), and L is the crack length in the material. Figure 13 shows the calculated energy release rates for PBN of the tested grain sizes. The curve fitted to the points follows the equation $G = .024223 * \ln(g) + .011832$, as a logarithmic curve is observed to be the most suited to describing it. The values thus calculated are similar to yet lower than those which have been calculated for graphene (~0.08)[41], as can be expected from this material. The relationship between the energy release rate and the grain size of PBN may be attributed to the

weakness induced from the grain boundary. As the weakness introduced in the mechanical properties through grain boundaries simultaneously decreases the energy release rate for smaller grain sizes, where more grain boundaries are present.

4 Conclusions

Hexagonal boron nitride is one of the 2D materials currently garnering attention; as evidenced by the growing technologies based on boron nitride, especially in environments untenable for many materials such as continuous exposure high temperature and abrasion. From our study based on the molecular dynamics simulations, it can be shown that polycrystalline boron nitride exhibits mechanical properties both similar and dissimilar to polycrystalline graphene. The general relationship of grain size with strength, strain, toughness, Young's Modulus, and energy release rate have been determined with high-fidelity logarithm-base fitting curves. Our findings have established that strength, toughness, Young's Modulus, and energy release rate all have a declining trend along with a decrease of grain size, while the ultimate strain increases at grain sizes decrease. These properties stem from the heterogeneity of BN, and the effect of this heterogeneity on the behavior of grain boundaries, and this influences the failure mechanisms seen in PBN. Judging from these results, and supported by previous works, it can be concluded that polycrystalline boron nitride, although weaker than pristine boron nitride, still has remarkable mechanical properties which can be tuned through control of the average grain size of the material. This tunability allows for the designing of customized materials such as polymer composites with added stability from PBN, able to be controlled for specific environments.

Author Information

Corresponding authors: Xianqiao Wang (xqwang@uga.edu)

Author Contributions: MB performs the simulations, XW designs the simulations, and MB and XW write the manuscript.

Notes: The authors declare no competing financial interest.

Acknowledgements

MB and XW acknowledge support from the National Science Foundation and University of Georgia (UGA) Research Foundation. Calculations are performed at the UGA Advanced Computing Resource Centre.

References

1. P. R. Cantwell, M. Tang, S. J. Dillon, J. Luo, G. S. Rohrer and M. P. Harmer, *Acta Mater*, 2014, **62**, 1-48.
2. C. Jasiukiewicz, T. Paszkiewicz and S. Wolski, *Phys Status Solidi B*, 2010, **247**, 1201-1206.
3. M. L. Liao, T. W. Lian and S. P. Ju, *Advanced Materials and Nanotechnology*, 2012, **700**, 125-128.
4. B. Mortazavi and G. Cuniberti, *Rsc Adv*, 2014, **4**, 19137-19143.
5. E. S. Oh, *Mater Lett*, 2010, **64**, 859-862.
6. G. J. Slotman and A. Fasolino, *J Phys-Condens Mat*, 2013, **25**, 045009.
7. B. Mortazavi and Y. Remond, *Physica E*, 2012, **44**, 1846-1852.
8. W. Sekkal, B. Bouhafs, H. Aourag and M. Certier, *J Phys-Condens Mat*, 1998, **10**, 4975-4984.
9. C. Sevik, A. Kinaci, J. B. Haskins and T. Cagin, *Phys Rev B*, 2011, **84**, 085409
10. H. N. Liu and C. H. Turner, *Phys Chem Chem Phys*, 2014, **16**, 22853-22860.
11. A. Lyalin, A. Nakayama, K. Uosaki and T. Taketsugu, *J Phys Chem C*, 2013, **117**, 21359-21370.
12. Y. C. Wang, J. M. Lu, S. P. Ju, H. L. Chen, H. T. Chen, J. S. Lin, J. Y. Hsieh, H. W. Yang and L. F. Huang, *J Nanosci Nanotechno*, 2013, **13**, 1256-1260.
13. Z. M. Shi, X. G. Zhao and X. R. Huang, *J Mater Chem C*, 2013, **1**, 6890-6898.
14. X. L. Li, X. J. Wu, X. C. Zeng and J. L. Yang, *Acs Nano*, 2012, **6**, 4104-4112.
15. P. Miro, M. Audiffred and T. Heine, *Chem Soc Rev*, 2014, **43**, 6537-6554.
16. Y. D. Kuang, S. Q. Shi, P. K. L. Chan and C. Y. Chen, *Comp Mater Sci*, 2010, **50**, 645-650.
17. K. B. Dhungana and R. Pati, *Sensors-Basel*, 2014, **14**, 17655-17685.
18. J. M. Zhang, S. F. Wang, K. W. Xu and V. Ji, *J Nanosci Nanotechno*, 2010, **10**, 840-846.
19. M. Griebel and J. Hamaekers, *Comp Mater Sci*, 2007, **39**, 502-517.
20. A. Bagri, S. P. Kim, R. S. Ruoff and V. B. Shenoy, *Nano Lett*, 2011, **11**, 3917-3921.
21. A. J. Cao and J. M. Qu, *J Appl Phys*, 2012, **111**, 053529.
22. T. H. Liu, S. C. Lee, C. W. Pao and C. C. Chang, *Carbon*, 2014, **73**, 432-442.
23. O. V. Yazyev and S. G. Louie, *Nature Materials*, 2010, **9**, 806-809.
24. J. F. Zhang and J. J. Zhao, *Carbon*, 2013, **55**, 151-159.
25. H. J. Zhang, G. Lee, C. Gong, L. Colombo and K. Cho, *J Phys Chem C*, 2014, **118**, 2338-2343.
26. L. A. Jauregui, H. L. Cao, W. Wu, Q. K. Yu and Y. P. Chen, *Solid State Commun*, 2011, **151**, 1100-1104.
27. Y. Y. Liu, X. L. Zou and B. I. Yakobson, *Acs Nano*, 2012, **6**, 7053-7058.
28. H. Zhang, Z. Duan, X. N. Zhang, C. Liu, J. F. Zhang and J. J. Zhao, *Phys Chem Chem Phys*, 2013, **15**, 11794-11799.
29. J. F. Zhang, J. J. Zhao and J. P. Lu, *Acs Nano*, 2012, **6**, 2704-2711.

30. P. Y. Huang, C. S. Ruiz-Vargas, A. M. van der Zande, W. S. Whitney, M. P. Levendorf, J. W. Kevek, S. Garg, J. S. Alden, C. J. Hustedt, Y. Zhu, J. Park, P. L. McEuen and D. A. Muller, *Nature*, 2011, **469**, 389–392.
31. J. A. Baimova, L. Bo, S. V. Dmitriev, K. Zhou and A. A. Nazarov, *Epl-Europhys Lett*, 2013, **103**, 46001
32. B. Wang, Y. Puzyrev and S. T. Pantelides, *Carbon*, 2011, **49**, 3983-3988.
33. T. Zhang, X. Y. Li, S. Kadkhodaei and H. J. Gao, *Nano Lett*, 2012, **12**, 4605-4610.
34. H. Y. Cao, H. J. Xiang and X. G. Gong, *Solid State Commun*, 2012, **152**, 1807-1810.
35. D. R. Nutt and H. Weller, *J Chem Theory Comput*, 2009, **5**, 1877-1882.
36. M. Becton, X. W. Zeng and X. Q. Wang, *Carbon*, 2015, **86**, 338-349.
37. S. Plimpton, *J Comput Phys*, 1995, **117**, 1-19.
38. K. Matsunaga, C. Fisher and H. Matsubara, *Jpn J Appl Phys 2*, 2000, **39**, L48-L51.
39. M. Zhao, J. C. Li and Q. Jiang, *J Alloy Compd*, 2003, **361**, 160-164.
40. C. V. Thompson, *J Mater Res*, 1993, **8**, 237-238.
41. J. L. Tsai, S. H. Tzeng and Y. J. Tzou, *Int J Solids Struct*, 2010, **47**, 503-509.

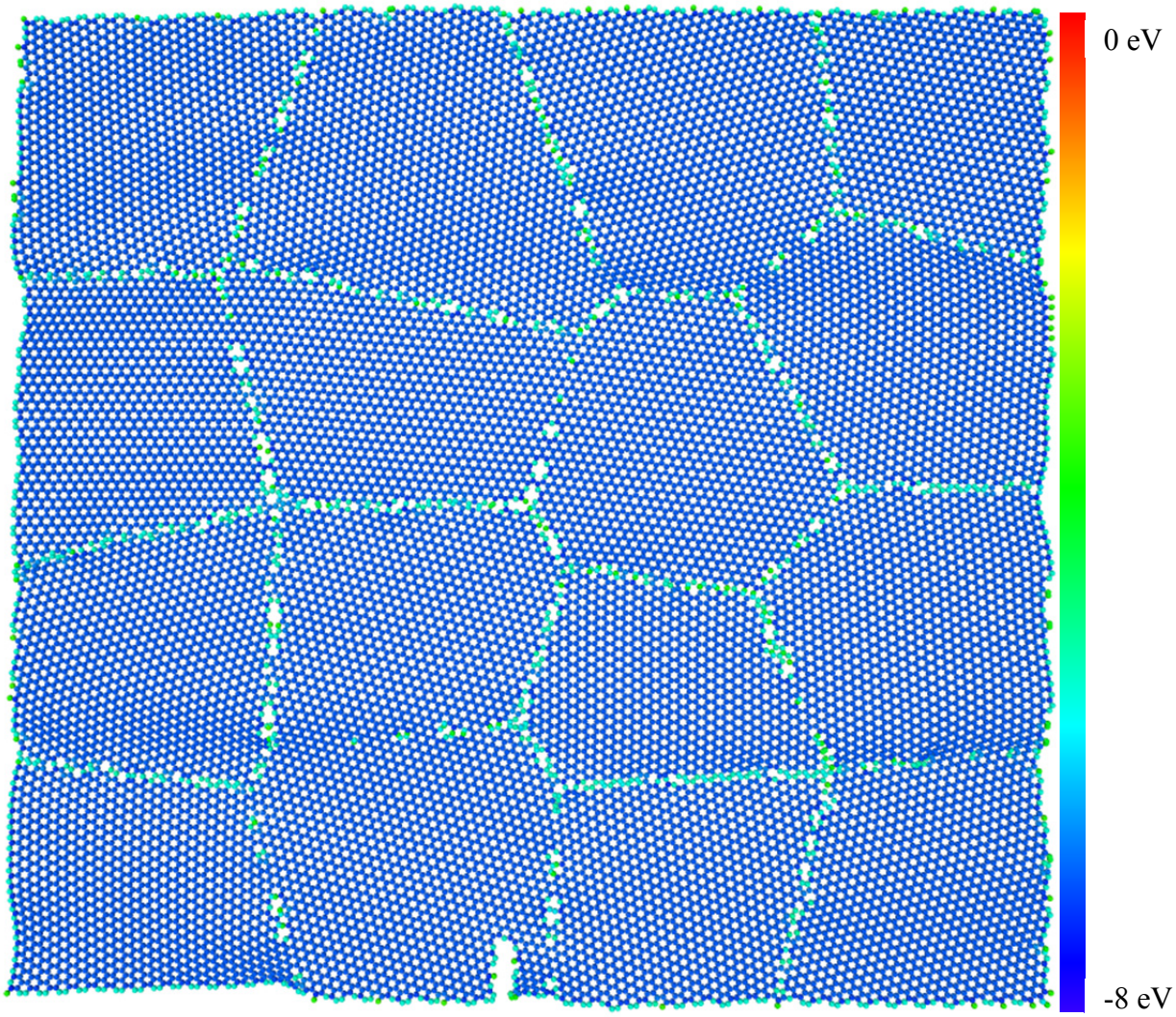

Figure 1: Representative image of 6 nm grain size PBN with 2 nm predefined crack. The atoms are colored with respect to potential energy in order to highlight the grain boundaries.

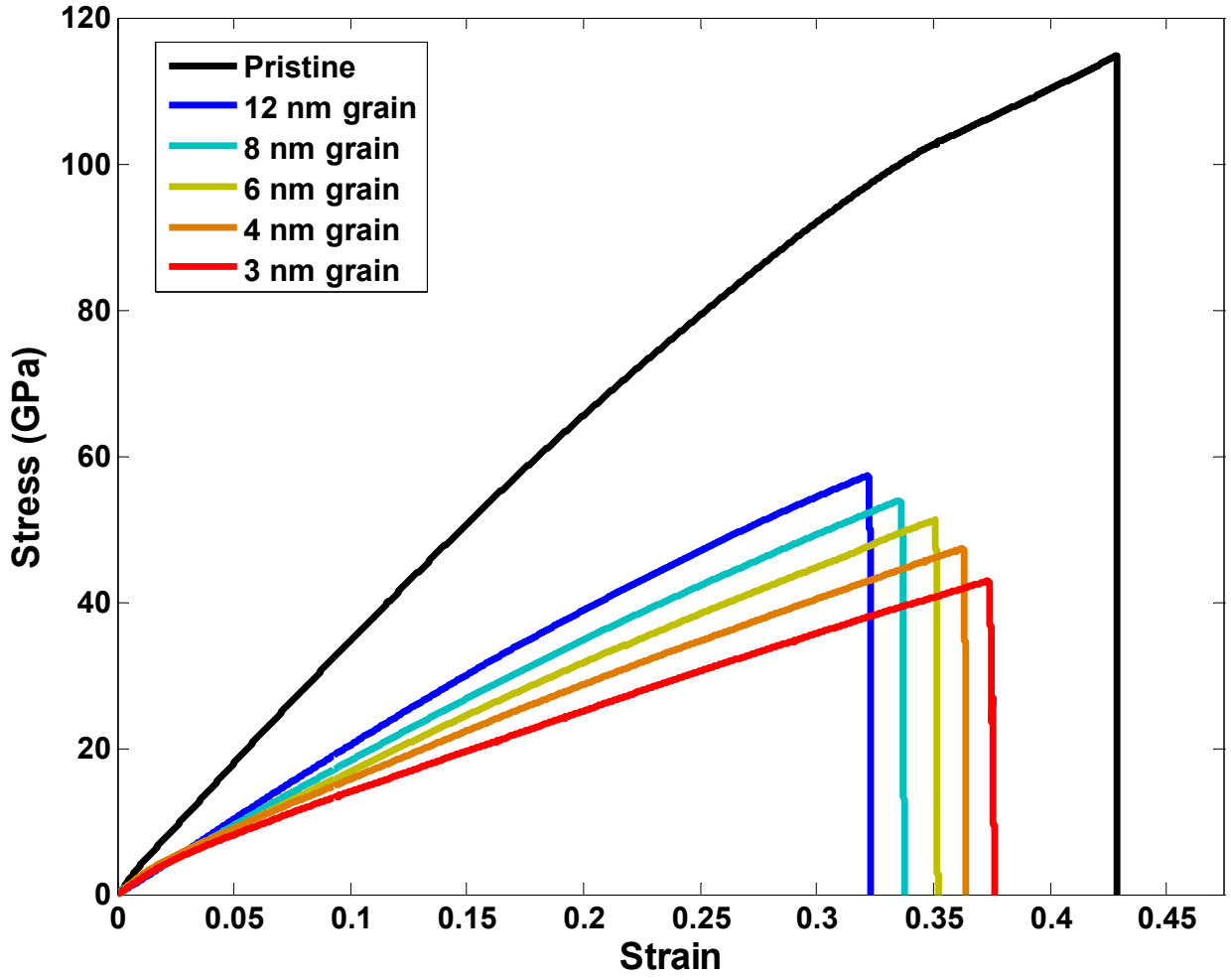

Figure 2: Stress-strain relationship for pristine BN and PBNs.

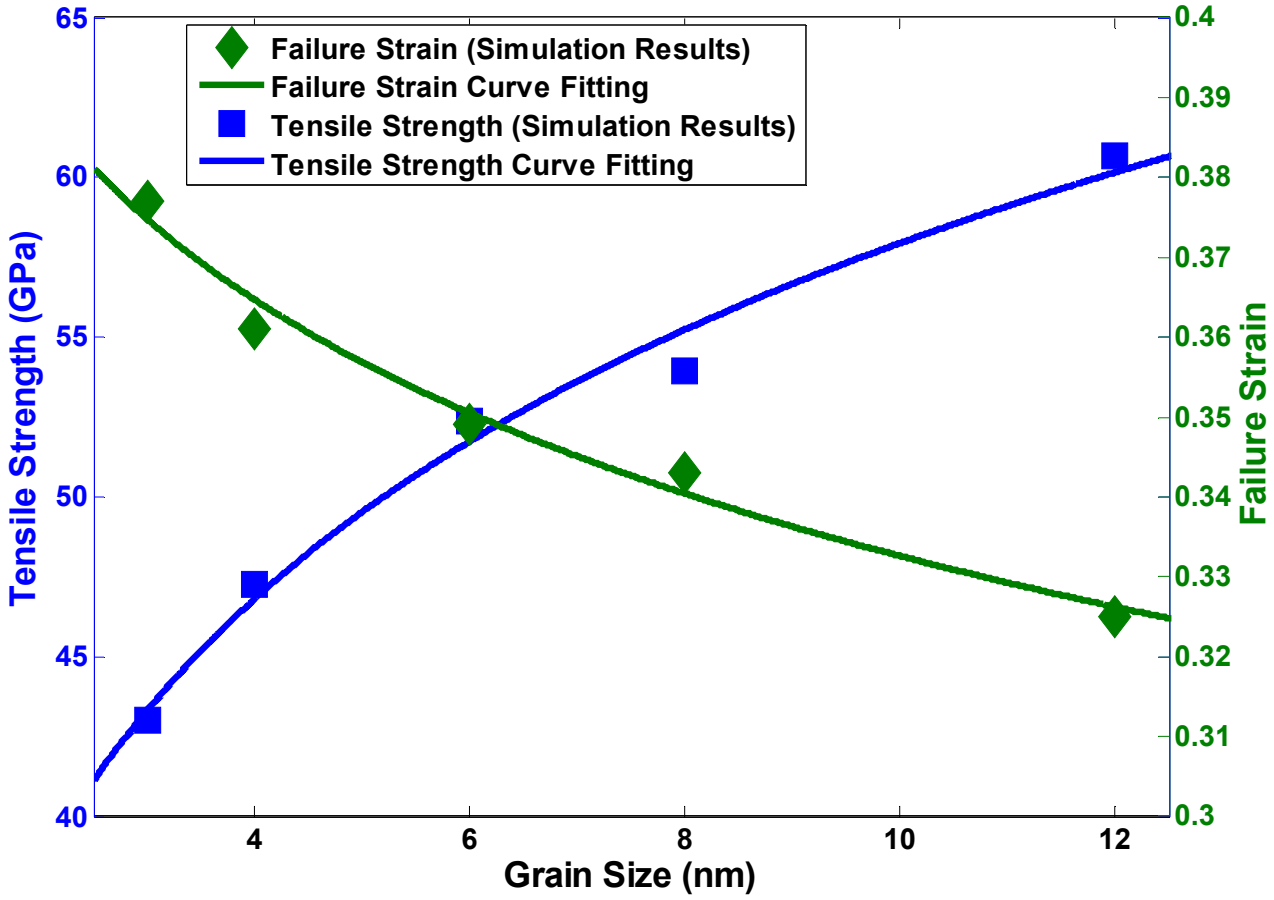

Figure 3: Relationship between grain size, tensile strength, and failure strain for PBN along with fitted curves to the data points.

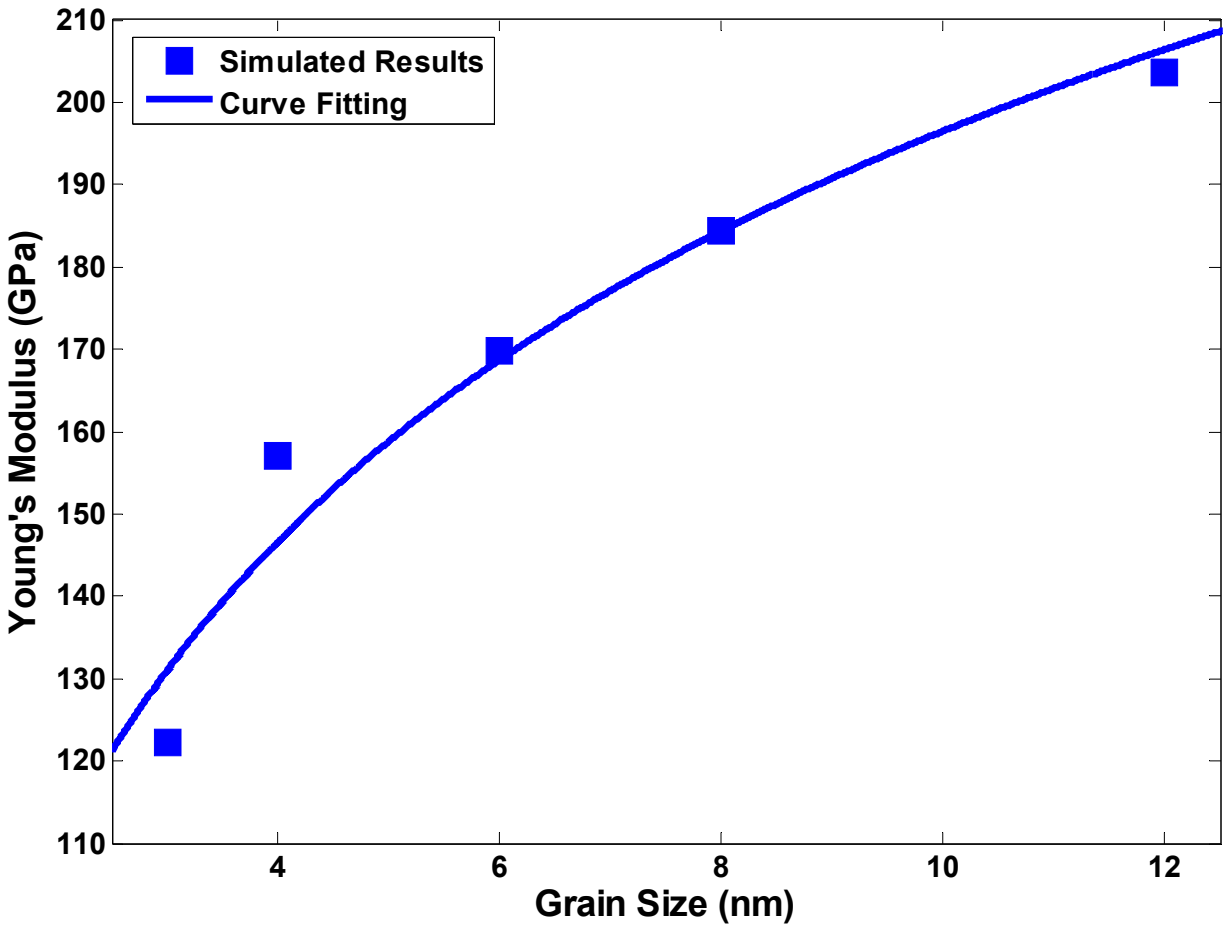

Figure 4: Relationship between grain size and Young's Modulus for PBN along with a fitted curve to the data points.

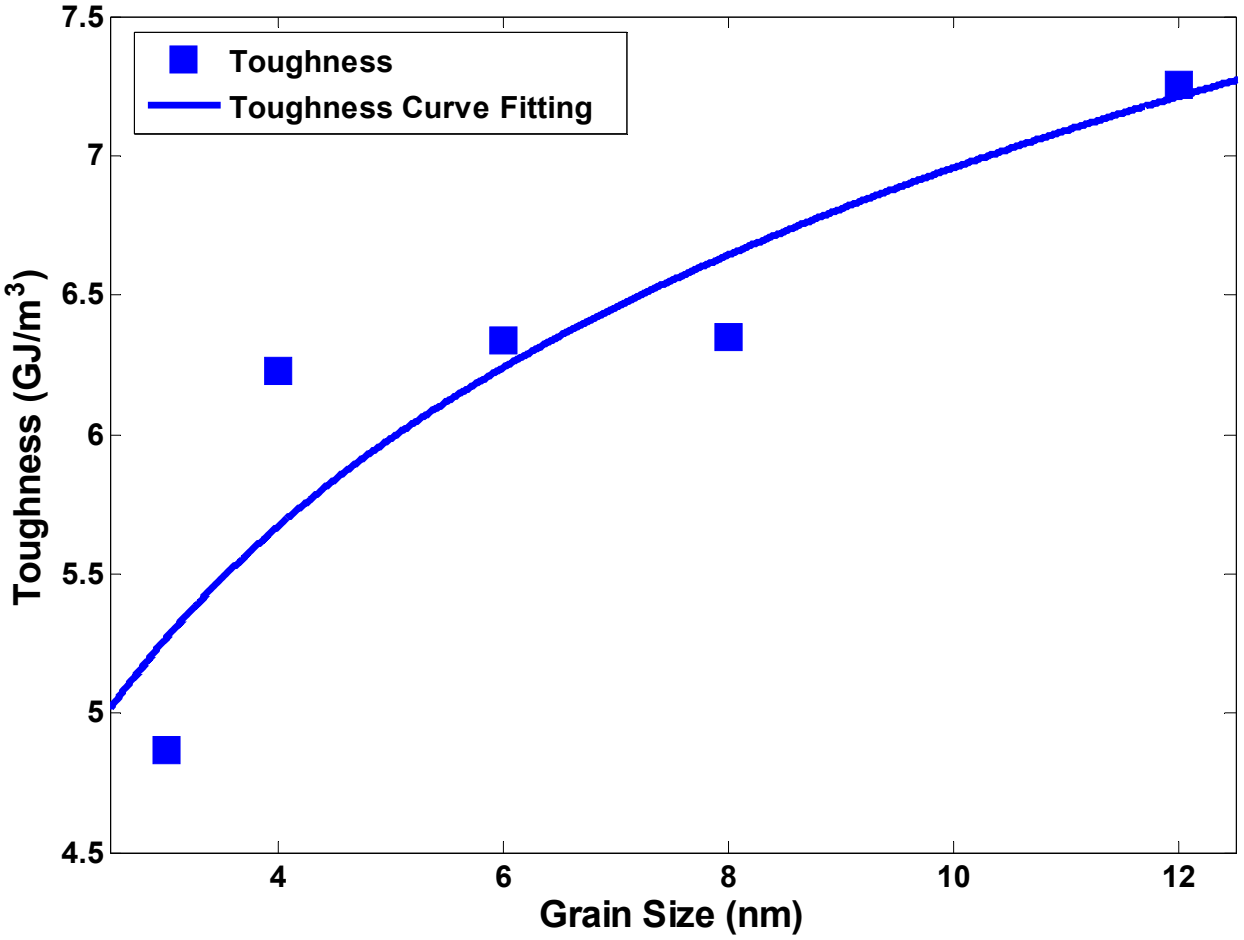

Figure 5: Relationship between grain size and toughness for PBN along with a fitted curve to the data points.

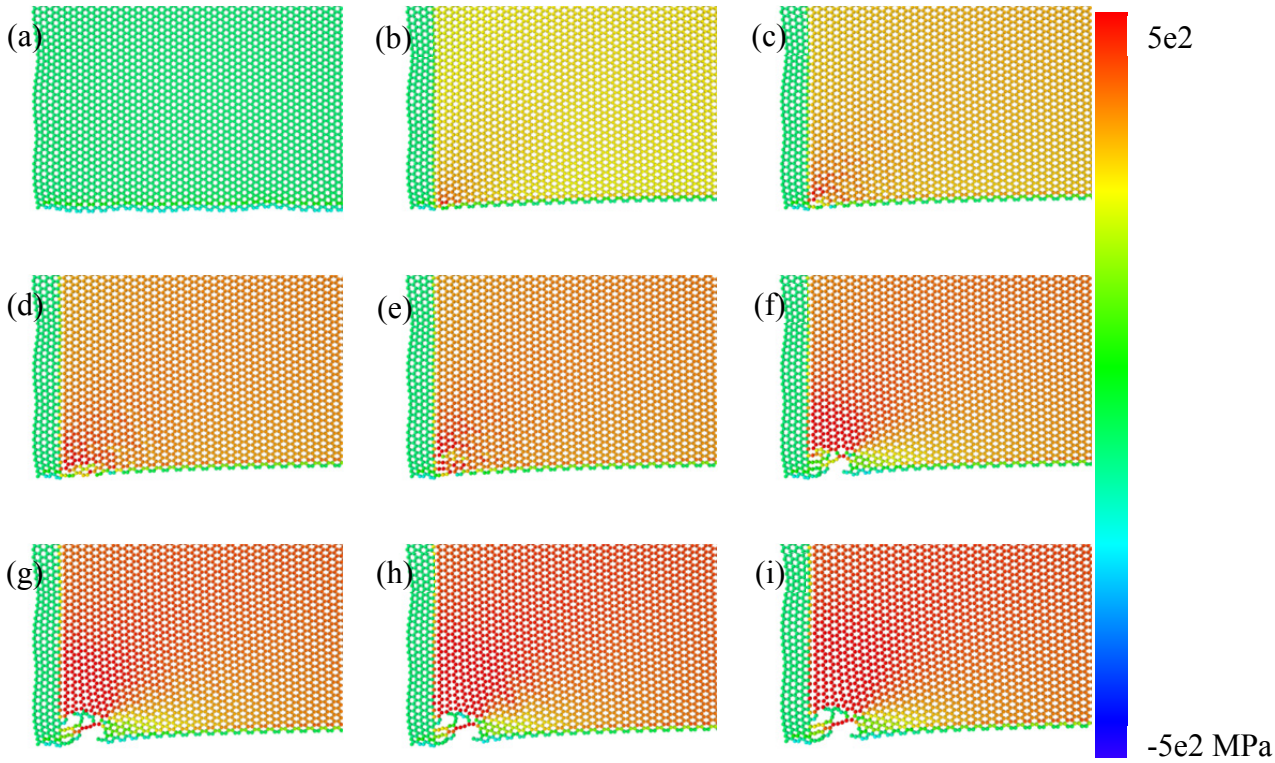

Figure 6: Stress of pristine BN leading up to fracture.

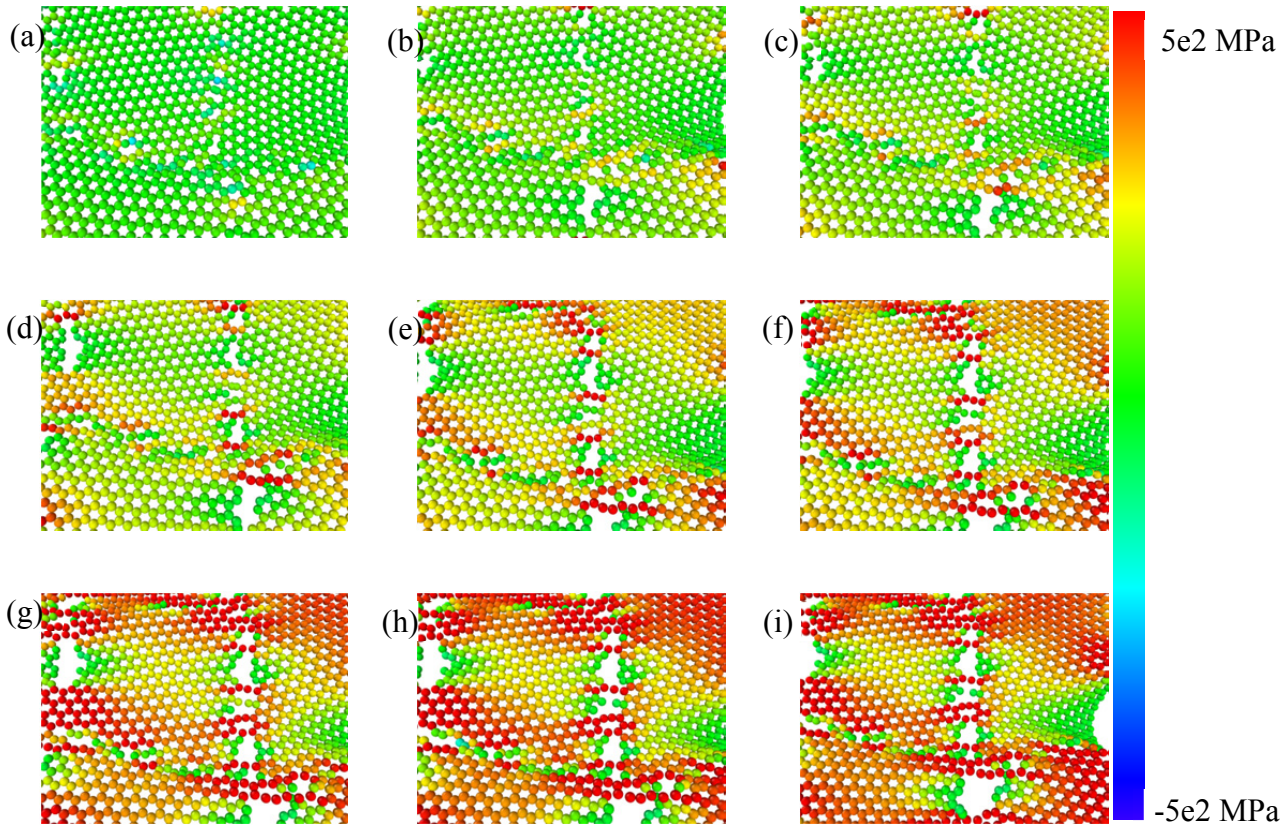

Figure 7: Stress of a single grain of 3 nm grain PBN leading up to fracture.

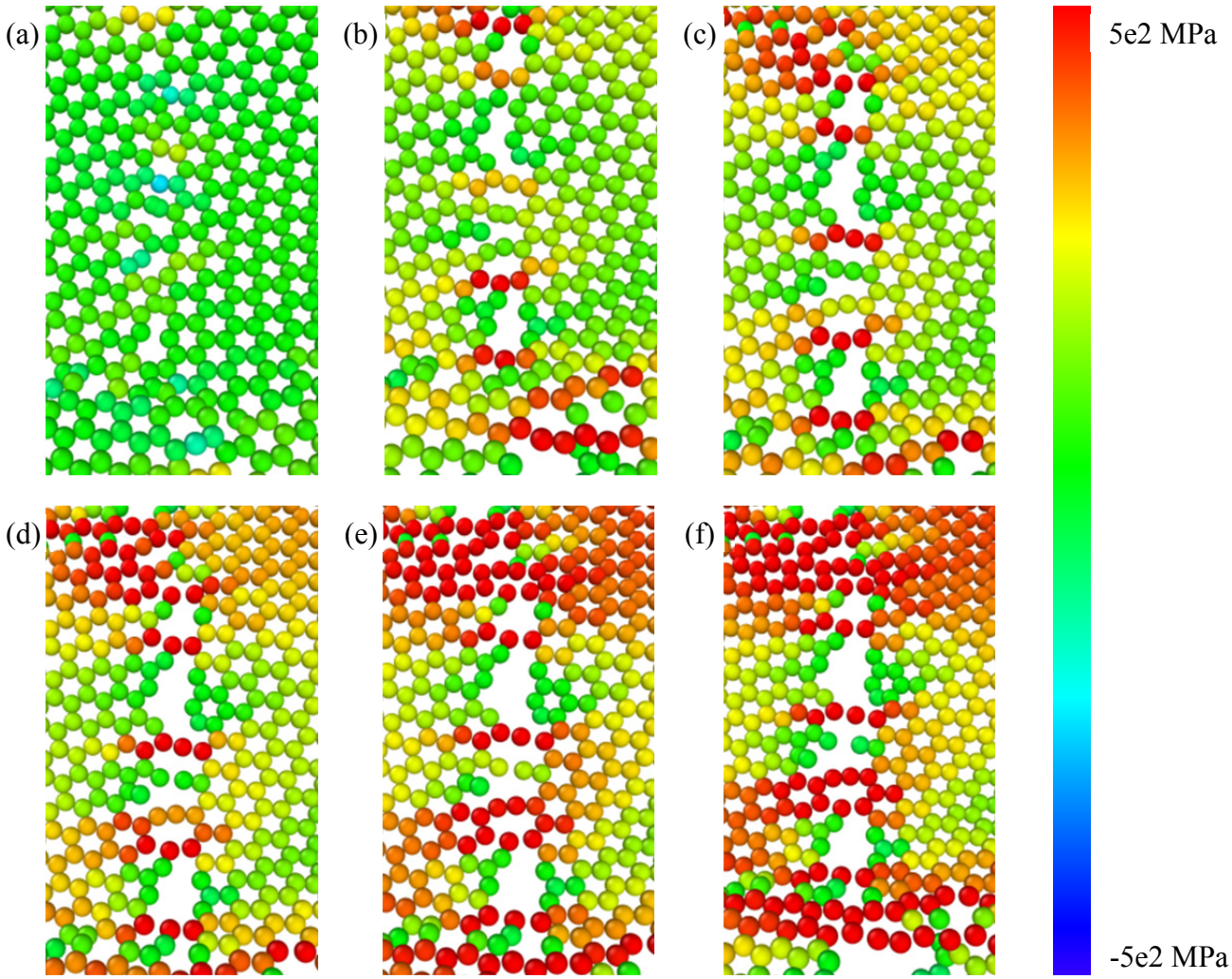

Figure 8: Close-up view of the stress of a portion of the grain boundary illustrated in Figure 7.

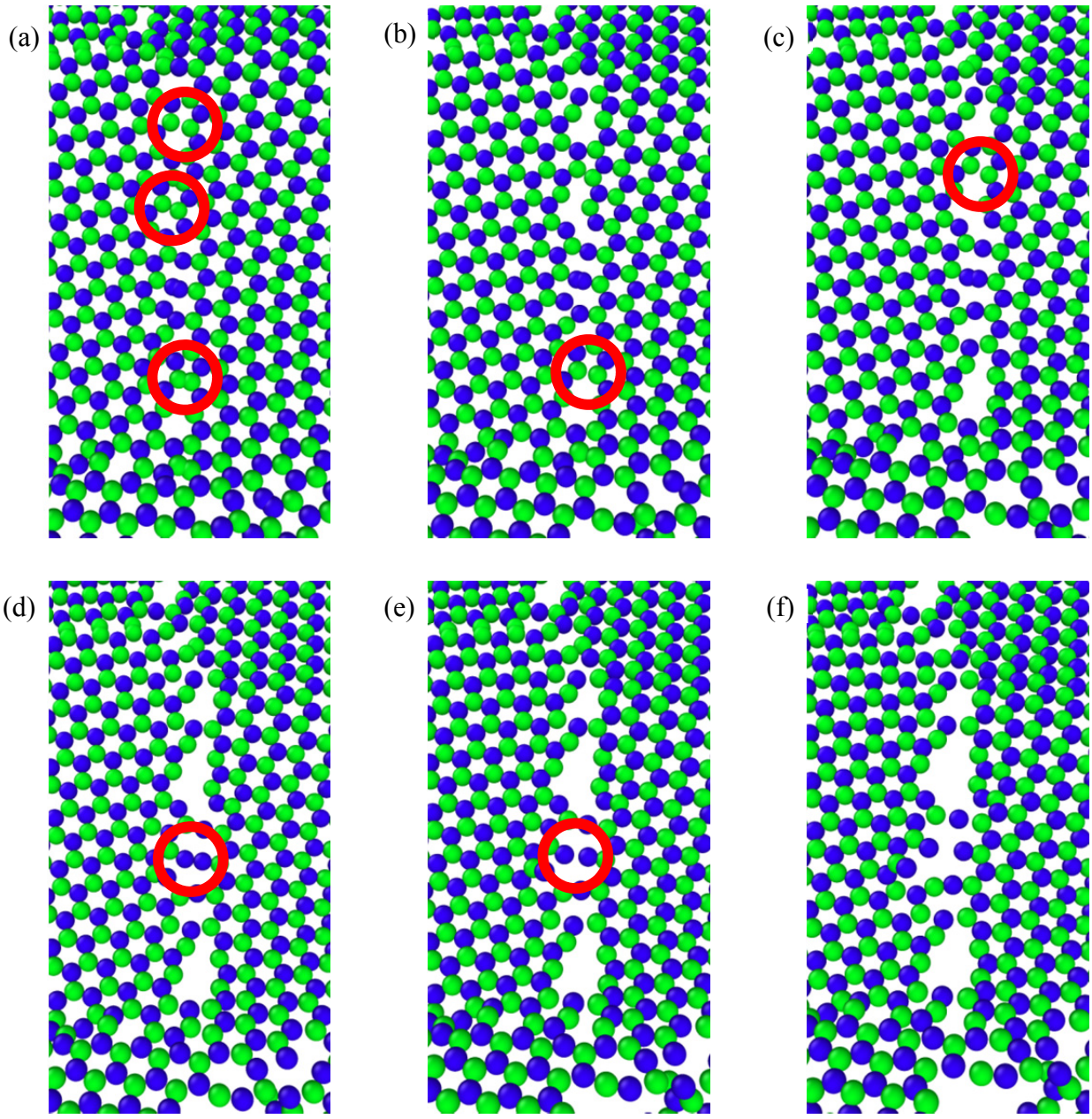

Figure 9: Close-up view of the atomic species of the grain boundary illustrated in Figure 8. In this image, blue is used for boron, and yellow for nitrogen.

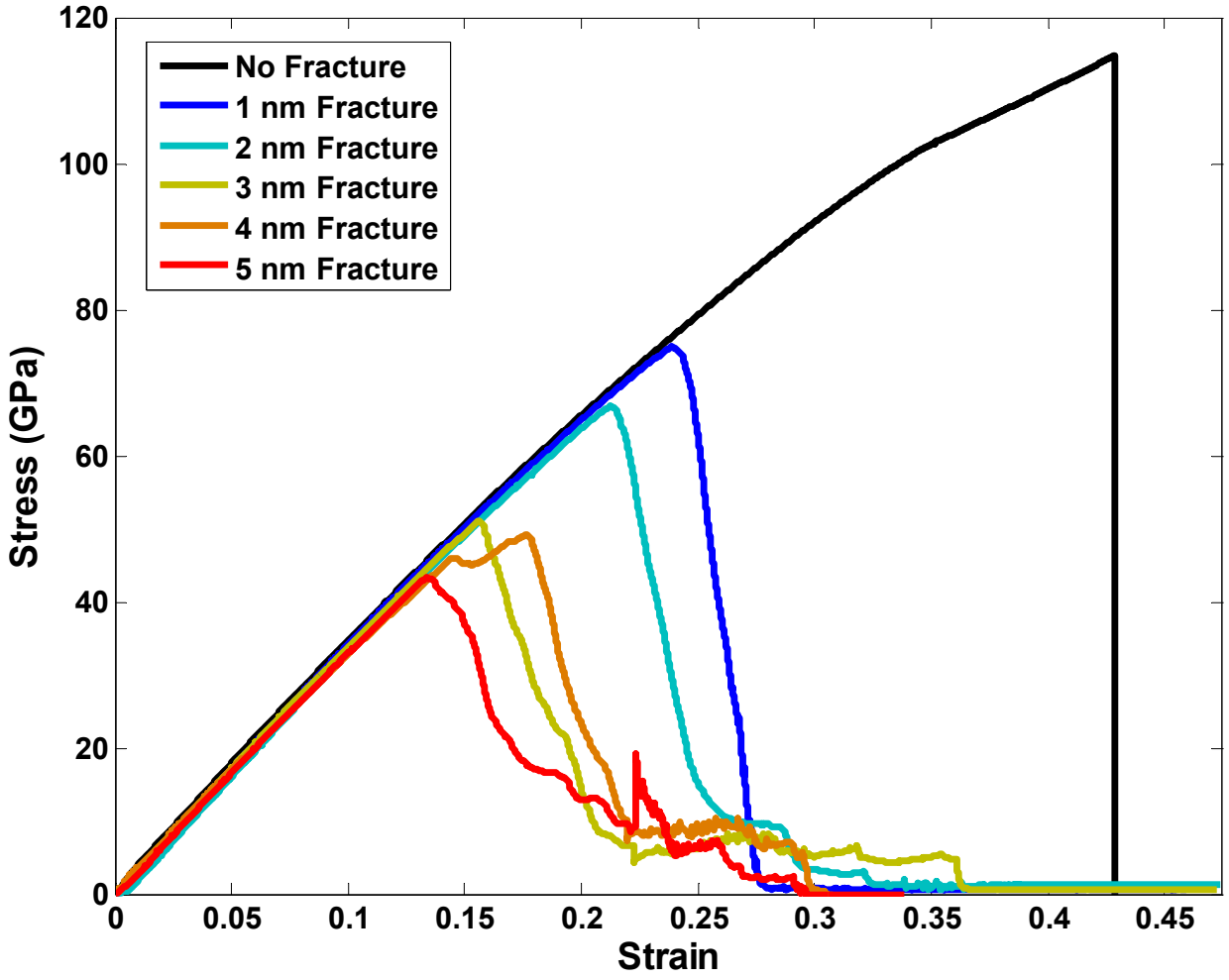

Figure 10: Stress-strain relationship for pristine BN with varying initial predefined crack lengths.

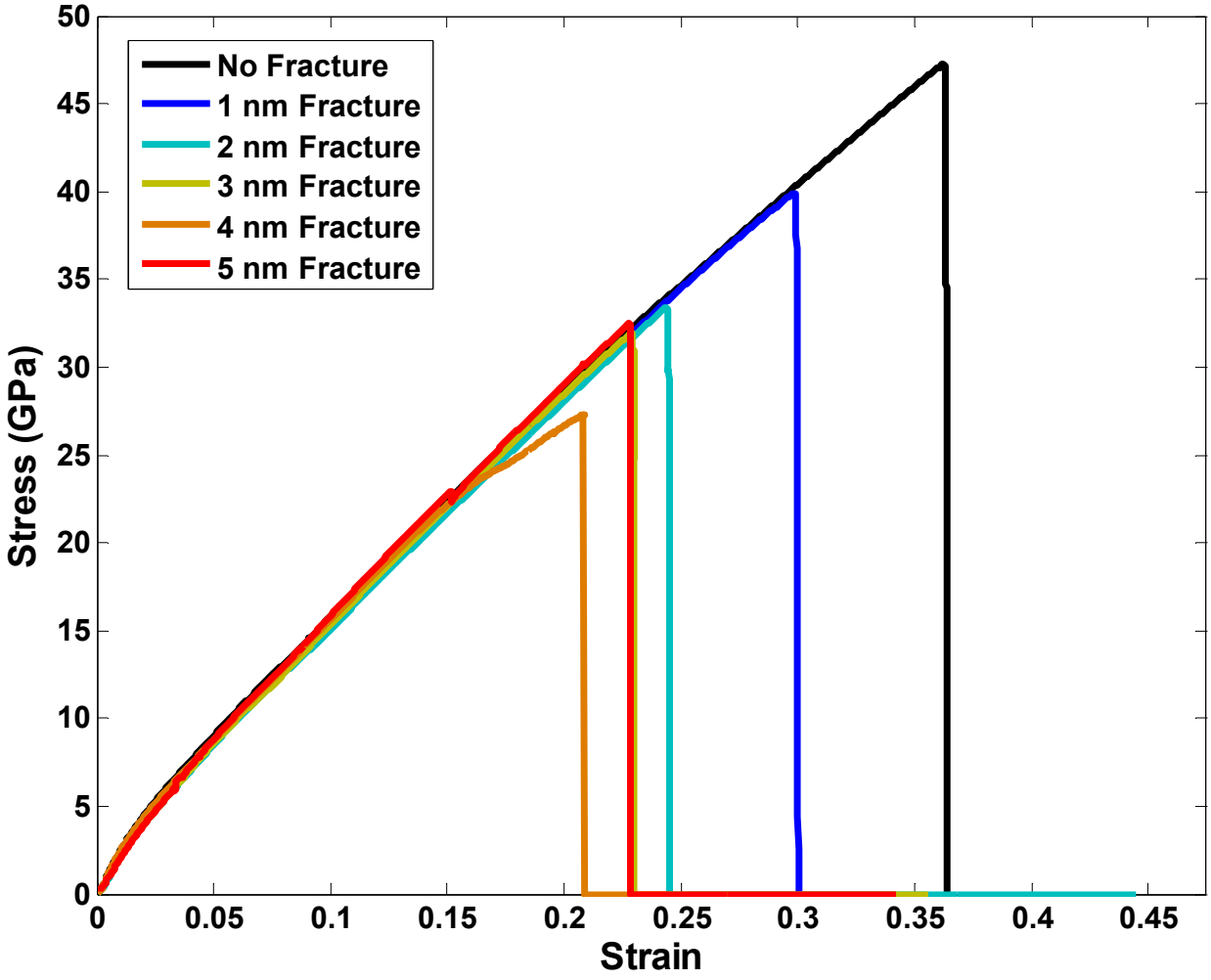

Figure 11: Stress-strain relationship for 4 nm PBN with varying initial predefined crack lengths.

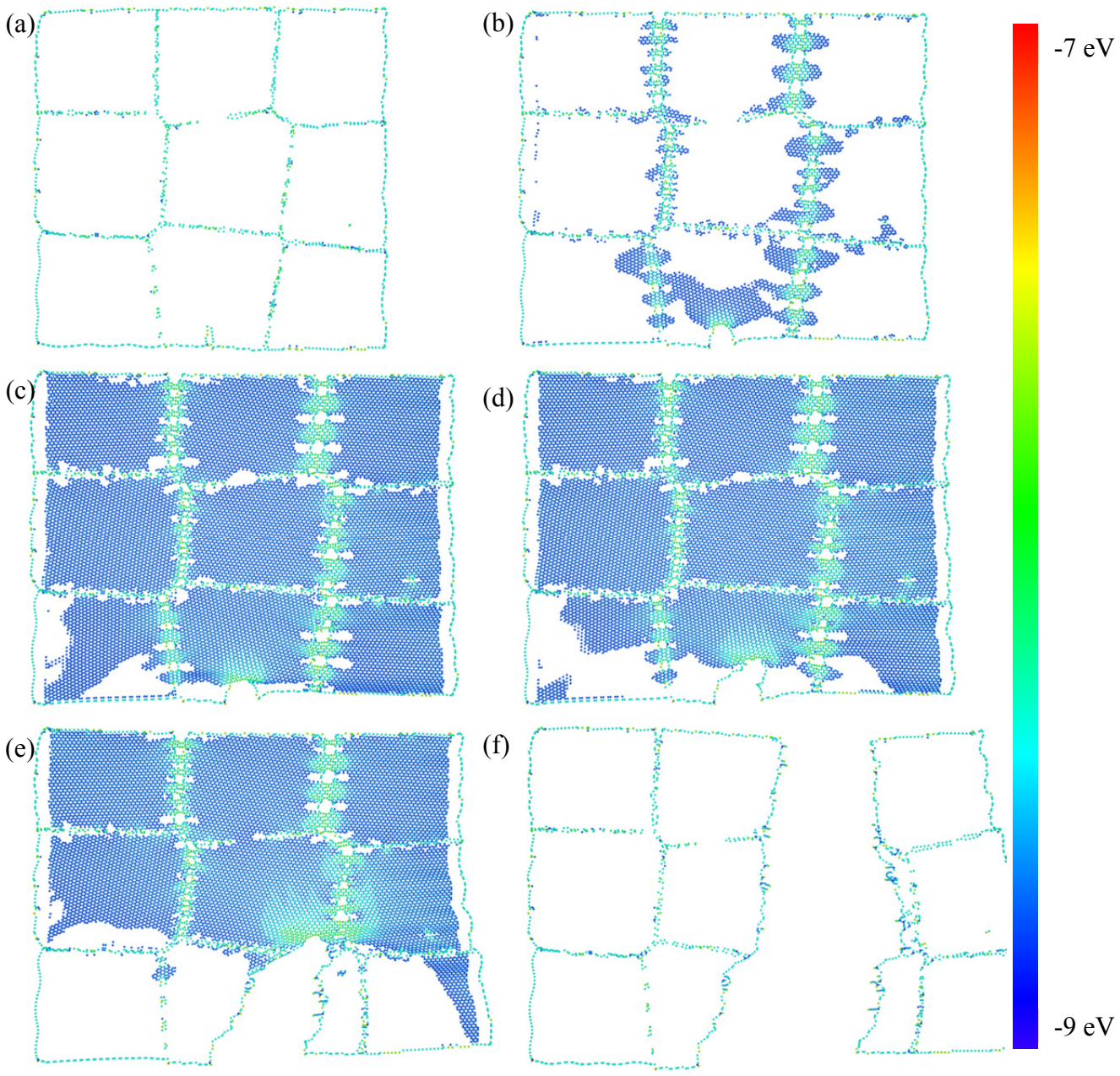

Figure 12: Potential energy plot of 8 nm grain size PBN with predefined crack during the tensile process. Only atoms from -7 to -9 eV are shown to better highlight grain boundaries, edges, and bond stretching.

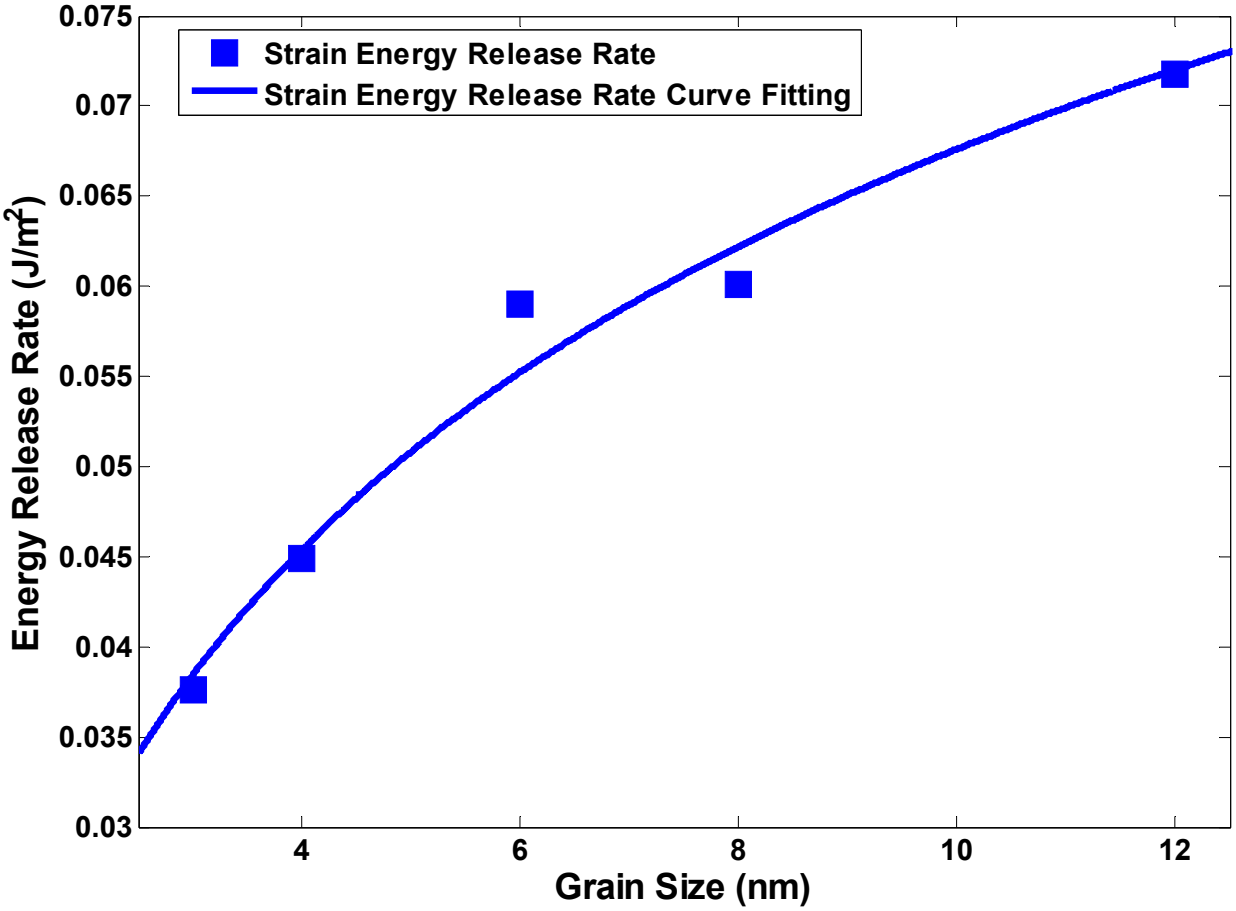

Figure 13: Energy release rate as a function of grain size for PBN, with a curve fitted to the data.